

# Downstream Extraction Line Polarimeter

Ken Moffeit  
SLAC, Stanford, CA

Presented at the Workshop on Polarization and Energy measurements at the ILC  
9-11 April 2008, DESY, Zeuthen, Germany

## Abstract

The Compton polarimeters situated in the electron and positron extraction lines downstream of the  $e^+e^-$  interaction region in the International Linear Collider are described in this paper.

## 1. Introduction

The downstream polarimeters in the extraction lines of the ILC are designed to operate with high precision from the Z-pole center of mass energy to the highest ILC energies available of 1 TeV. The polarimeter measurement will be performed by a Compton polarimeter chosen for several reasons:

- The physics of the scattering process is well understood in QED, with radiative corrections less than 0.1% [1];
- Detector backgrounds are easy to measure and correct for by using laser off pulses;
- Polarimetry data can be taken simultaneously with physics data;
- The Compton scattering rate is high and small statistical errors can be achieved in a short amount of time (sub-1% precision in one minute is feasible);
- The laser helicity can be selected on a pulse-by-pulse basis;
- The laser polarization is readily determined with 0.1% accuracy;
- Timing of the laser pulses can be varied to sample systematically all electron bunches in the train.

The ILC baseline design described in the Reference Design Report [2] has an electron-positron Interaction Point crossing angle of 14 mrad, which permits an extraction line downstream polarimeter measuring the polarization of the outgoing beam after the collision [3]. The luminosity-weighted depolarization from the electron-positron collisions is  $\sim 0.3\%$ , while the average depolarization of the outgoing beam to the extraction line is  $\sim 1\%$ . The extraction line optics is chosen to be focused at the Compton IP with the beam transport matrix designed to have a horizontal angular magnification of  $\sim -0.5$ . The beam polarization measured by the extraction line polarimeter is then very similar to the luminosity-weighted polarization. In non-colliding beams mode, the downstream polarimeter can measure the undisturbed beam as well, so that spin transport effects between the upstream polarimeter can be disentangled from the effects of the collisions.

Five bunch trains with 2,820 electron bunches ( $2 \cdot 10^{10}$  per bunch) in each train will occur at the ILC each second. Three low repetition rate lasers of 10 Hz each produces the light for collision at the Compton IP with three electron bunches of each train. The high power lasers give good signal-to-background ratio in the more difficult downstream environment with disrupted primary electrons and beamstrahlung photons present. The timing of the Compton laser pulses can be varied so as to sample systematically all electron bunches in the train and determine any variation of the beam polarization along the train. The three lasers will also permit continued operation while routine maintenance on a laser takes place.

An accuracy of  $(\Delta P_e / P_e) = 0.25\%$  should be achievable with systematic error contributions given in Table 1. The largest contribution comes from detector analyzing power of 0.2%.

<b>Uncertainty</b>	$\delta P / P$
Detector Analyzing Power	0.2%
Detector Linearity	0.1%
Laser Polarization	0.1%
Electronic Noise and Background Subtraction	0.05%
<b>TOTAL</b>	<b>0.25%</b>

**Table 1:** Systematic error contributions to the downstream extraction line polarization measurement.

## 2. Extraction Line Optics

The disrupted electron (positron) beam is transported straight ahead into the extraction line clearing the positron (electron) beam line elements of the incoming beam. The disrupted beam is focused by quadrupoles (beginning at  $z=6$  meters) at the Compton IP located at the center of the polarimeter chicane 147.682 meters downstream of the  $e^+e^-$  IR. The disrupted beam beta functions and vertical dispersion are shown in Figure 1.

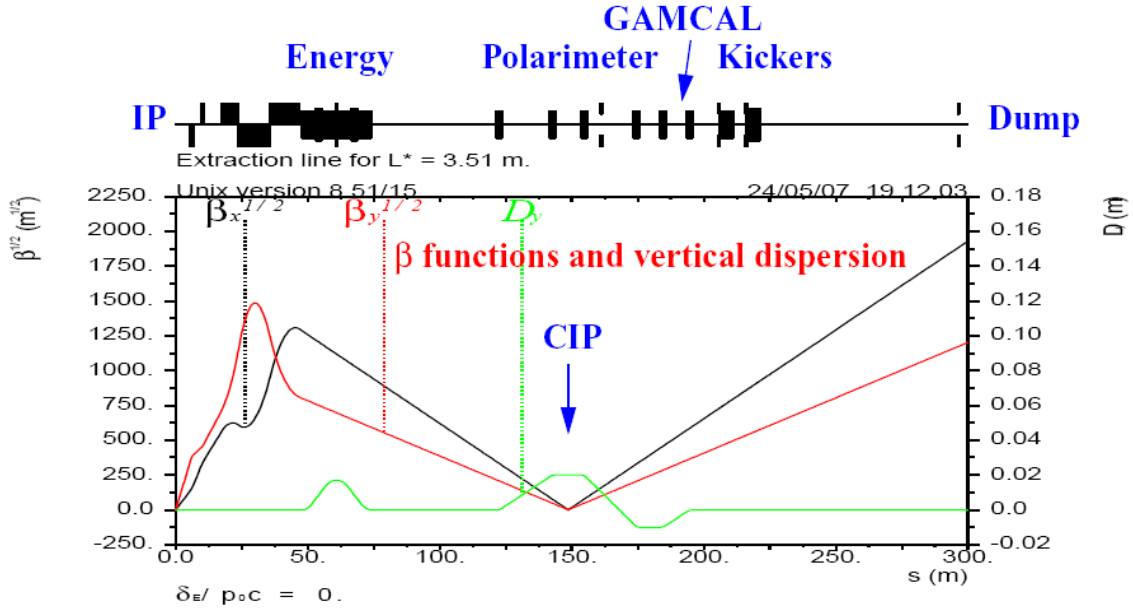


**Figure 1:** Disrupted beta functions and vertical dispersion in the 14 mrad extraction line. Electron-positron interaction point is at  $s = 0$  and the Compton interaction point is located at  $s=147.682$  meters.

The downstream Compton Interaction Point is located at the secondary focus in the middle of a 4-magnet chicane having bends in the vertical plane with 20 mm dispersion. There is no net bend angle at the Compton IP with respect to the beam direction at the  $e^+e^-$  interaction point, and the angle tolerance needs to be within 50 micro-radians. A schematic drawing of the extraction line is shown in Figure 2.

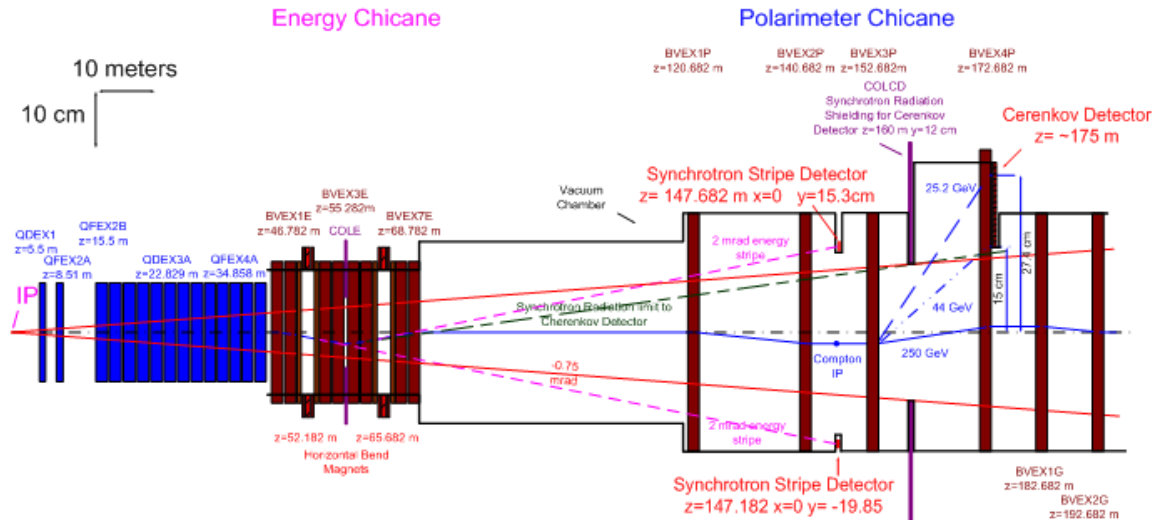


**Figure 2:** Diagram of the Energy Chicane and Polarimeter Chicane in the 14 mrad extraction line. Longitudinal distances given are from the IP. Also shown in red is the 0.75 mrad beam stay-clear from the IP.

The cost for the downstream polarimeter chicane given in the ILC baseline has four magnets with the same deflection in each magnet system. A proposal to modify the polarimeter chicane in the ILC 14 mrad extraction line to a six-magnet chicane was presented to the ILC in March 2007 [3]. The additional two magnets after the Compton detector shown in figures 1 and 2 allow the third and fourth magnets of the polarimeter chicane to be operated at higher field to deflect the Compton electrons further from the beam line and return the beam to the nominal trajectory. Both the 4-magnet and 6-magnet polarimeter chicanes are shown in the RDR. The proposal to change the extraction line to the six-magnet chicane has not been formally accepted in the baseline by the ILC management.

**Recommendation: Modify the extraction line polarimeter chicane from a 4-magnet chicane to a 6-magnet chicane to allow the Compton electrons to be deflected further from the disrupted beam line.**

### 3. Laser System

The laser room is on the surface above the Compton polarimeter chicane in the extraction line. It is 10m by 10m by 3m and contains a room for electronics, a gowning room and clean room housing the laser and optical systems. Diagrams of the laser room and the laser source systems are shown in Figure 3 and 4.

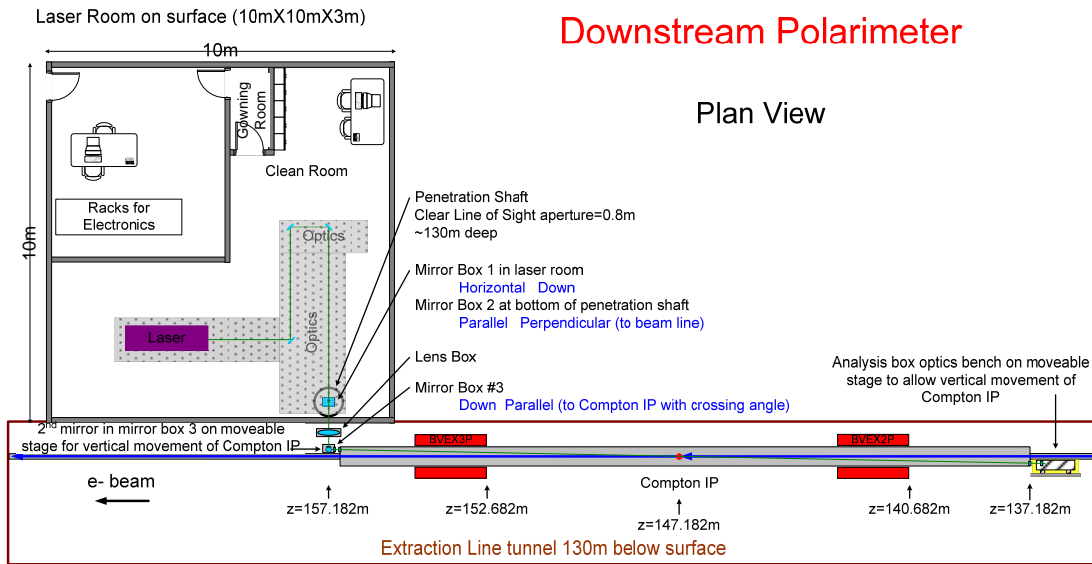


**Figure 3:** Diagram of Laser Room showing its location on the surface above the extraction tunnel. The penetration is located above an alcove off the electron beam tunnel.

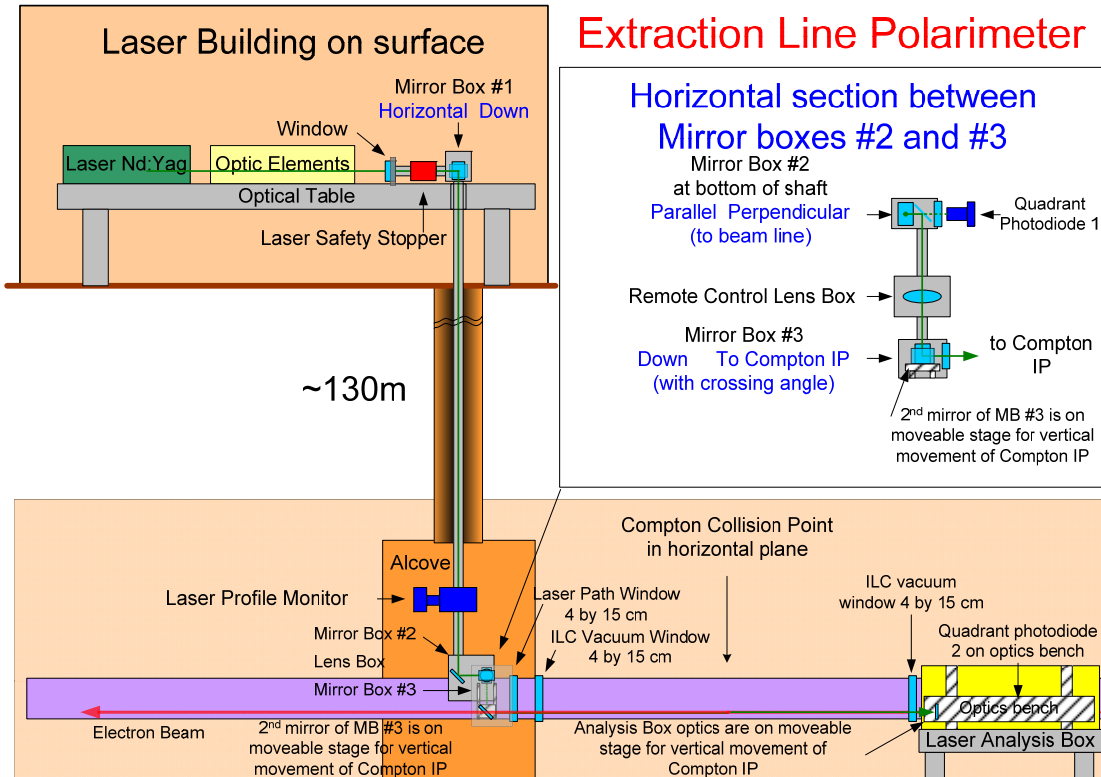


**Figure 4:** Schematic of the systems of the downstream extraction line Compton laser light source showing the laser and optics, the transport line to the Compton Interaction Point in the tunnel underground and the Analysis Box. The penetration is located above an alcove off the electron beam tunnel.

### 3.1 Laser

Three frequency doubled Nd:YAG (Neodymium:Yttrium-Aluminum-Garnet) lasers will be used with a wavelength of 532 nm (2.33 eV). Each of the three lasers will operate at 10 Hz. Compton collisions occur on one bunch of each of the 5 Hz bunch trains. The other 5 Hz will be used for diagnostic information. Each laser has a solid Nd:YAG rod, which is pumped into an excited state by flash lamps, and the resulting atomic transitions produce 1064 nm photons. The laser beam passes through a frequency-doubling crystal, which uses a nonlinear optics phenomenon to combine two 1064 nm photon states into a single 532 nm state. The resulting beam of 1064 nm and 532 nm photons passes through an infrared separator to assure that there are only 532 nm photons in the laser beam as it enters the optics bench optical components. The laser pulse energy delivered to the Compton IP is ~100 mJ. The duration of the Q-switched laser pulse is ~6 nanoseconds. The light emerges from the laser linearly polarized.

A possible available commercial laser is the Continuum Powerlite Model 8000 shown in figure 5: 10Hz; 600 mJ at 532nm; 6ns pulse width (FWHM) [4].

**Continuum**  
An Excel Technology Company  
**Powerlite™ Precision II 8000**



**POWERLITE™ 8000 SPECIFICATIONS**

DESCRIPTION	8000	8010	8020	8030	8050
Repetition Rate (Hz)	10	10	20	30	50
Energy (mJ)					
1064 nm	1200	1650	1200	650	550
532 <sup>1</sup> nm	600	800	550	300	210
355 <sup>2</sup> nm	310	450	300	150	95
266 nm	120	150	80	50	30
Pulsewidth <sup>3</sup> (nsec)					
1064 nm	6-8	6-8	6-8	7-9	7-9
532 nm	5-7	5-7	5-7	6-8	6-8
355 nm	5-7	5-7	5-7	6-8	6-8
266 nm	5-7	5-7	5-7	6-8	6-8
Linewidth <sup>4</sup> (cm <sup>-1</sup> )					
Standard	1	1	1	1	1
Injection Seeded, SLM	0.003	0.003	0.003	0.003	0.003
Divergence <sup>5</sup> (mrad)	0.45	0.45	0.45	0.5	0.5
Beam Pointing Stability <sup>6</sup> (±μrad)	30	30	30	30	30
Warm up time <sup>7</sup> (<min)	5	5	5	5	5
Jitter <sup>8</sup> (±ns)					
Unseeded	0.5	0.5	0.5	0.5	0.5
Seeded	1.0	1.0	1.0	1.0	1.0
Energy Stability <sup>9</sup> (±%)					
1064 nm	2.5; 0.8	2.5; 0.8	2.5; 0.8	3.0; 1.0	3.0; 1.0
532 nm	3.5; 1.2	3.5; 1.2	3.5; 1.2	4.5; 1.5	4.5; 1.5
355 nm	4.0; 1.3	4.0; 1.3	4.0; 1.3	5.0; 1.7	5.0; 1.7
266 nm	10; 3.3	10; 3.3	10; 3.3	10; 3.3	10; 3.3
Power Drift <sup>10</sup> (±%)					
1064 nm	3.0	3.0	3.0	5.0	5.0
532 nm	5.0	5.0	5.0	6.0	7.0
355 nm	5.0	5.0	5.0	6.0	8.0
266 nm	8.0	8.0	8.0	8.0	8.0
Beam Spatial Profile (Fit to Gaussian) <sup>11</sup>					
Horizontal Near Field (<1m)	0.7	0.7	0.7	0.7	0.7
Far Field (∞)	0.95	0.95	0.95	0.95	0.95
Max Deviation from fitted Gaussian <sup>12</sup> (±%)					
Near Field (<1m)	40	40	40	40	40
Service Requirements					
220 or 240 VAC, single Φ	10A	11A	16A	15A	21A
208 VAC, 3 Φ	6A	7A	10A	9A	13A
Water GPM at 40-60 PSI	1-2	1-2	1-2	1-2	1-2

**Figure 5:** Picture showing Continuum Powerlite Model 8000 along with the specification for different models.

The Compton laser light source provides high-intensity pulses of circularly polarized light at the Compton Interaction Point, CIP. The laser beam must be transported with minimal loss of polarization from the laser source to the collision point with the electrons. The circular polarization of the light must be well measured and monitored to achieve an uncertainty in the circular polarization of the laser light at the Compton IP of 0.1%. The light source for the extraction line Compton polarimeter described here is similar to that used in the SLD experiment at the SLAC Linear Collider [5].

### 3.2 Laser Room Optical Bench

Beams from three 10Hz rep rate lasers are combined using polarizing beam splitters and Pockels cells as shown in figure 6. This provides 15 Hz of Compton collisions with 3 independent bunches in a given train. Adjusting the Q-switch timing of the lasers allows different bunches in the train to be sampled to monitor polarization differences along the train. Three laser modules provide robust fail-safe laser operation, allowing continued polarimeter measurements if one module fails. There are five primary laser control systems described below: i) Manual Intensity Control, ii) Remote Intensity Control, iii) Pulse Length Control, iv) Remote Steering Control, and v) Remote Polarization Control.

The polarizing beam splitters and first two Pockels cells allow matching the laser beam polarization to the first polarizer of the Pulse Length Control system.

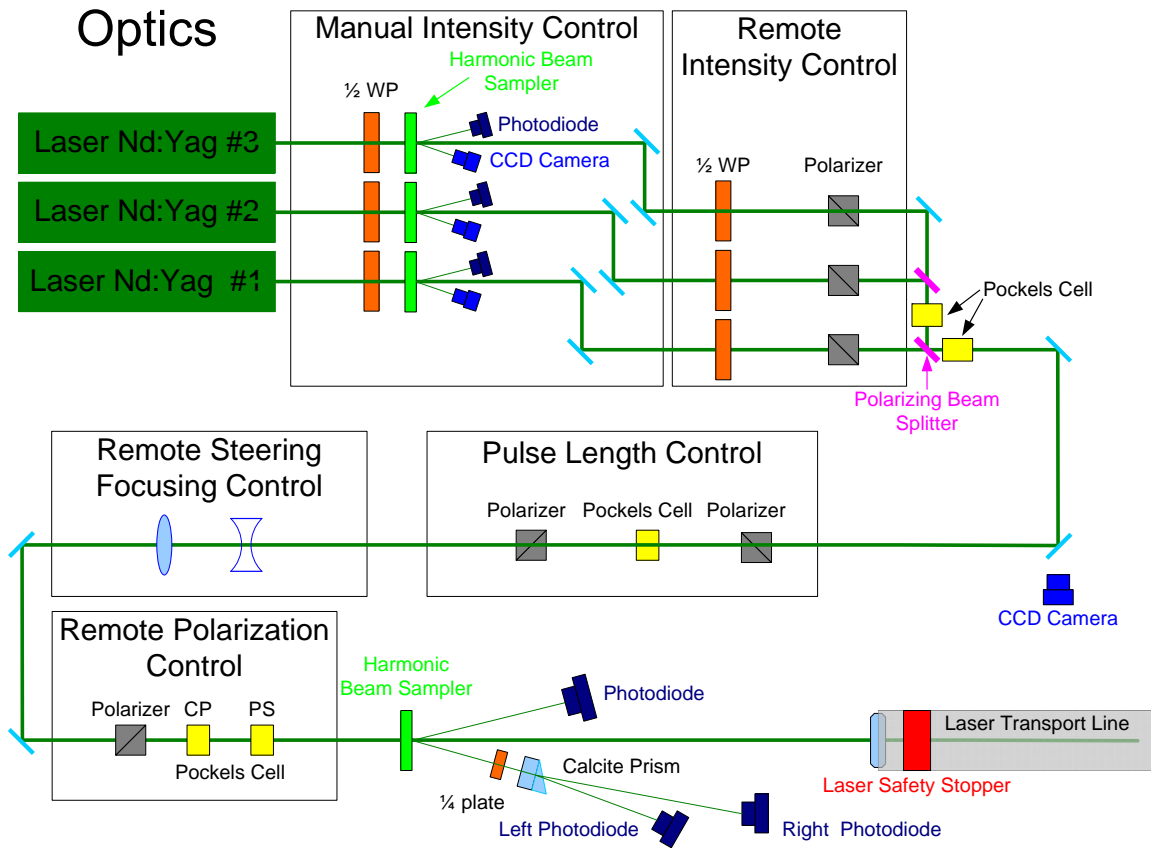


**Figure 6:** Diagram of the Compton source laser optical bench layout.

A number of Pockels cells are used in the optical systems to rotate linear polarization by 90 degrees, obtain short pulses and to generate circular polarization of the laser light. The Pockels cell was invented by Friedrich Pockels in 1893. A Pockels cell alters the polarization state of light passing through it when an applied voltage induces birefringence changes in an electro-optic crystal such as KD\*P. When used in conjunction with polarizers, these cells can function as optical switches, or laser Q-switches. It is a voltage-dependent optical compensator inducing different phase shifts along different axes. The fast axis has the smallest phase shift, and the axis perpendicular is the slow axis and has the largest phase shift. The axes of the Pockels cell are aligned 45 degrees to the linear polarization of the incident light. The specifications for the Pockels cell include the high voltages that correspond to a quarter-wave or half-wave phase shift for the wavelength of the incident light. Circularly polarized light is obtained by setting a voltage on the electrodes of the Pockels cell corresponding to a quarter-wave shift. Changing the sign of the voltage allows one to switch from right-circularly polarized light to left-circularly polarized light. The type of Pockels cell used in the SLD Compton Laser System for generating circular polarization is shown in Figure 7.

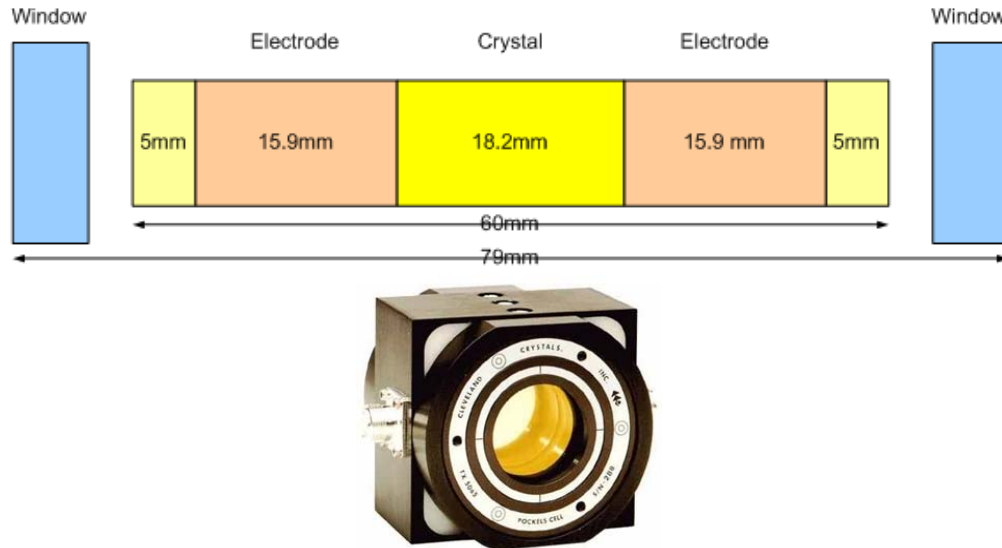


**Figure 7:** Cleveland Crystals Model TX3460 Pockels cell.

### 3.2.1 Manual Laser Intensity Control

A manually adjusted  $\frac{1}{2}$ -wave plate, in conjunction with a linear polarizer, attenuates the beam to the desired intensity to avoid damaging optical components on the bench and in the transport line. Photodiodes monitor the output of the laser from a small (1%) transmitted part of the beam generated by a harmonic beam sampler. If the output drops below the dynamic range of the Remote Intensity Control the operator manually adjusts the first  $\frac{1}{2}$ -wave plate or does maintenance on the laser, e.g. changes flash lamps. A mirror pair for each of the three lasers allows for steering and positioning of the laser beams so they are on the same path when they are merged. (If it is determined that there are significant relative steering drifts between the lasers, a steering feedback can be implemented using these mirror pairs.).

### 3.2.2 Remote Intensity Control

The Adjustable Remote Intensity Control consists of a remotely adjustable  $\frac{1}{2}$ - wave plate and linear polarizer and is used to remotely adjust the laser beam intensity to maintain the desired light intensity at the Compton IP.

### 3.2.3 Laser Pulse Length

A Pockels Cell is sandwiched between two crossed linear polarizers. A fast pulser drives the Pockels Cell at the  $\frac{1}{2}$ -wave plate voltage thereby rotating the linear polarization 90 degrees. The second crossed linear polarizer then accepts the laser light rotated and filters the non-rotated light. A narrow laser pulse length of  $\sim < 2$  nsec can be achieved. This narrow laser pulse ensures that only a single bunch of the electron beam pulse train is in collision, and reduces laser power in the transport optics to minimize the risk of optics damage. The timing of the Q-switched laser pulse and the fast pulser with respect to the electron beam pulse allows the polarization of each bunch of the electron beam pulse train to be measured. (We will also investigate using a laser with a short pulse length of  $\sim 50$ -100ps, in which case the laser pulse length system will not be needed.)

### 3.2.4 Remote Steering and Focusing Control

The beam is expanded to 2-cm diameter to reduce the intensity on the optics and provide a collimated beam through the transport line to the Compton IP, ~130m underground. The second lens in the beam expander is mounted on an XYZ stage to allow remote steering and focusing control. Using the Laser Position Monitor looking at quadrant photodiode behind Mirror Box 2 (see Figure 4) for the steering diagnostic, the laser spot at the Lens Box can be maintained allowing correction for thermal effects on the optics of the transport line. The distance between the lenses can be adjusted to control the collimated beam profile in the transport line and optimize the focusing of the laser beam at the Compton IP.

### 3.2.5 Remote Polarization Control

A linear polarizer ensures 100% linear polarization as the laser beam enters a set of two Pockels cells to create circularly polarized light at the Compton Interaction Point. The first Pockels cell labeled CP produces the desired circular polarization and is operated pulse-by-pulse with a pseudo-random helicity selection. It is referred to as the Circular Polarization Pockels cell because when the linear polarized light passes through it, it becomes almost completely circularly polarized. The principle axes of this cell are tilted by  $45^\circ$  with respect to the linear polarization of the incident light. The second Pockels cell provides phase adjustment so the beam can be made nearly 100% circularly polarized at the Compton IP. The phase adjustment is needed to compensate for phase shifts from the optical elements in the transport line. The principle axes of this cell are either parallel or perpendicular to the axes defined by the initial linear light. Thus the retarding axes of the PS Pockels cell are aligned  $45^\circ$  with respect to the axes of the CP Pockels cell.

By varying the voltages on the CP and PS Pockels cells maximal circular polarization ( $\sim 99.9\%$ ) at the Compton IP can be achieved. The electric field vector after the PS cell in Jones Matrix notation is given by:

$$|E\rangle = \begin{vmatrix} E_x \\ E_y \end{vmatrix} = \begin{vmatrix} \sin\left(\frac{\delta_{CP}}{2}\right) \\ e^{i(\pi/2 + \delta_{PS})} \cos\left(\frac{\delta_{CP}}{2}\right) \end{vmatrix} \quad (2)$$

where

$$\delta_{CP} = \frac{V_{CP}}{V_{CP}^{\lambda/4}} \cdot \frac{\pi}{2}$$

$$\delta_{PS} = \frac{V_{PS}}{V_{PS}^{\lambda/4}} \cdot \frac{\pi}{2}$$

and  $V_{CP}$  ( $V_{PS}$ ) is the CP (PS) Pockels Cell voltage,  $V_{CP}^{\lambda/4}$  ( $V_{PS}^{\lambda/4}$ ) is the CP (PS) quarter-wave voltage.  $V_{CP}$  controls the relative amplitudes of the  $E_x$  and  $E_y$  components and  $V_{PS}$  controls their relative phase. Hence, arbitrary elliptical polarization can be generated

with this configuration. The Stokes parameters for the laser polarization following the PS cell are:

$$\begin{aligned}
s_1 &= \cos \left( \frac{\delta_{CP}}{2} \right) = \frac{X - Y}{X + Y} \\
s_2 &= \sin(\delta_{CP}) \sin(\delta_{PS}) = \frac{U - V}{U + V} \\
s_3 &= \sin(\delta_{CP}) \cos(\delta_{PS}) = \frac{R - L}{R + L}
\end{aligned} \tag{3}$$

$$(s_1^2 + s_2^2) + s_3^2 = L^2 + C^2 = 1 \tag{4}$$

where  $s_1$  and  $s_2$  describe the linear polarization components and  $s_3$  is the circular polarization. For polarized light, the linear and circular polarization components add in quadrature to 1.

The CP and PS Pockels cells allow for compensating imperfections in the polarization Pockels cells and for phase shifts in downstream optics before the Compton IP. The circular polarization at the Compton IP is given by:

$$\begin{aligned}
s_3(CIP) &= \sin(\delta_{CP} + \delta_{CP}^{CIP}) \cos(\delta_{PS} + \delta_{PS}^{CIP}) \\
&= \sin \left( \frac{V_{CP} + \delta V_{CP}^{CIP}}{V_{CP}^{\lambda/4}} \cdot \frac{\pi}{2} \right) \cos \left( \frac{V_{PS} + \delta V_{PS}^{CIP}}{V_{PS}^{\lambda/4}} \cdot \frac{\pi}{2} \right)
\end{aligned} \tag{5}$$

where  $\delta_{CP}^{CIP}$  and  $\delta_{PS}^{CIP}$  describe the Pockels cell imperfections and phase shifts in the laser transport optics.

### 3.2.6 Laser Room Polarization Diagnostics

After exiting the PS Pockels cell, the beam is separated by a harmonic beam sampler giving two diagnostic beams at 10 degrees to the primary beam (each with ~1% of the intensity of the primary beam), while the primary beam continues into the laser transport line. One of the beams from the harmonic beam sampler is directed into a photodiode to monitor the laser intensity. The other beam enters a helicity filter consisting of a quarter-wave plate and calcite prism. The calcite prism separates the two perpendicular light polarization components and directs them into two photodiodes. These photodiodes monitor the circular polarization of the light,  $P_\gamma$ , as it enters the transport system through the following relation

$$P_\gamma = \frac{R - L}{R + L}, \tag{1}$$

where  $R, L$  are the (appropriately normalized) signals of the *Right, Left* photodiodes.

The crystal of a calcite prism has an index of refraction of 1.49 (1.66) for linear polarization in (perpendicular to) the scattering plane. Figure 8 shows the calcite prism used in the SLD polarimeter laser system as a helicity filter.

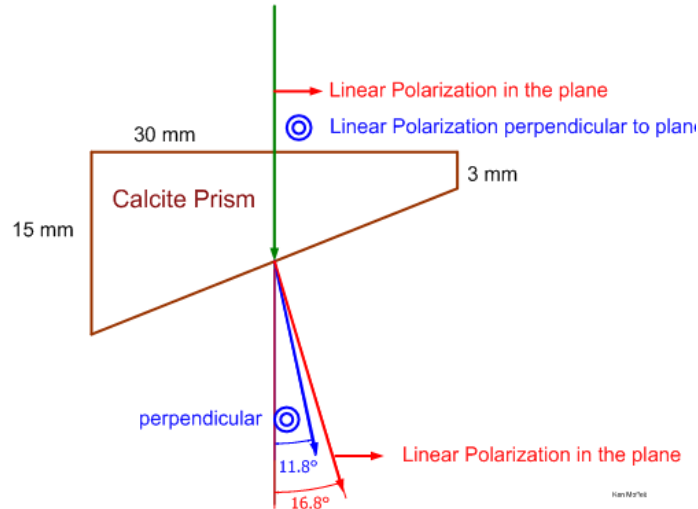


**Figure 8:** Diagram of Calcite Prism used in Helicity Filter.

### 3.3 Laser Transport Line to Compton IP

The transport line is designed to direct the laser light to the Compton interaction point with minimal alteration of the circular polarization. A schematic of the transport line is shown in Figure 3 and 4. The laser beam enters the transport line through a window of negligible birefringence and passes a fail-safe laser stopper located inside the laser building. The laser stopper is part of the laser safety system and does not allow laser light downstream when there is an unsafe condition, e.g. when the transport line is not at proper pressure. The transport line is filled with 3-5 psi overpressure of filtered nitrogen.

The laser beam is transported through three mirror boxes that contain matched circular polarization preserving pairs of mirrors. By using identical dielectric mirrors manufactured at the same time, any relative phase-delay shift for “s” and “p” polarization states (out-of-plane and in-plane polarization states) introduced by surface effects in the first mirror is exactly compensated for and removed by the second mirror in each Mirror Box. The two paired mirrors of each Mirror Box reflect the beam perpendicular to each other, resulting in a laser beam with “s” polarization at the first mirror becoming “p” polarized for the 2<sup>nd</sup> mirror and vice versa. For example, the first mirror of Mirror Box (1) reflects the beam 90 degrees in the horizontal and the second mirror reflects the beam 90 degrees to the vertical down the shaft.

The laser beam is deflected to the horizontal direction perpendicular to the electron beam line at Mirror Box (2). It then enters a Lens Box where it is focused at the Compton Interaction Point with a lens of ~11m focal length. The lens can be moved remotely in two directions perpendicular to the laser light direction allowing the laser beam to be



The laser light exits the extraction line vacuum through a 4 by 15 cm window, which is also chosen to have small birefringence. The laser light enters an Analysis Box where a 1/4-wave plate, calcite prism and (quadrant) photodiodes measure the circular polarization (see Figure 10). Quadrant photodiodes looking at a harmonic beam sampler are used for a 2<sup>nd</sup> remote steering feedback, using the Lens Box for the steering control. This, together with the steering feedback to stabilize the laser beam at the Lens Box, stabilizes the laser trajectory at the Compton IP. The optical elements in the analysis box are mounted on a moveable stage to accommodate vertical movement of the Compton IP (for operation with different electron beam energies).

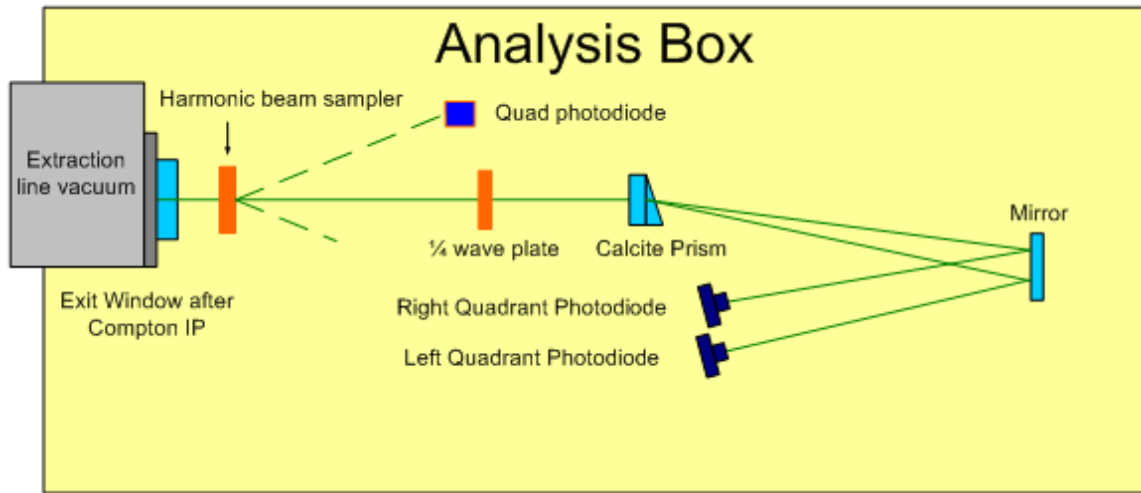


**Figure 10:** The Analysis Box optics located after the Compton IP.

### 3.4 Laser Beam Polarization Measurement at the Compton IP

The laser circular polarization is measured directly in the analysis box. However, the laser light passes through the exit window of the ILC vacuum chamber, which may change the circular polarization. The Compton asymmetry itself is therefore used to determine how to maximize the laser circular polarization at the Compton IP. The laser circular polarization,  $P_\gamma$ , at the Compton IP is determined from measurements of the photodiode signals of the laser beam and from Compton asymmetry measurements of the Compton-scattered beam electrons from the laser beam.

The laser polarization is directly measured before and after the Compton IP by measuring the amount of left-polarized and right-polarized light, using the *Right* and *Left* photodiodes that follow a helicity filter. The Compton asymmetry measurement is defined to be

$$A_{Compton} = \frac{N^{\rightarrow\rightarrow} - N^{\rightarrow\leftarrow}}{N^{\rightarrow\rightarrow} + N^{\rightarrow\leftarrow} - 2N^{off}} = AP_{Compton} \cdot P_e P_\gamma \quad (6)$$

where  $N^{\rightarrow\rightarrow}$  ( $N^{\rightarrow\leftarrow}$ ) is the detector signal for electron and laser photon spins aligned (anti-aligned);  $N^{off}$  is the detector signal with electron beam present, but no laser beam;

$AP_{Compton}$  is the analyzing power calculated from the Compton cross section and the detector response function;  $P_e$  is the electron beam longitudinal polarization.

The *Right* ( $PD^+$ ) and *Left* ( $PD^-$ ) photodiode signals and the measured Compton asymmetry ( $A_{Compton}$ ), are well-approximated by the following formulae:

$$PD^\pm = \frac{G^\pm}{2} \cdot \left[ 1 \pm \sin\left(\frac{V_{CP} + \delta V_{CP}^T}{V_{\lambda/4}^{CP}} \cdot \frac{\pi}{2}\right) \cos\left(\frac{V_{PS} + \delta V_{PS}^T}{V_{\lambda/4}^{PS}} \cdot \frac{\pi}{2}\right) + u \right]$$

$$A_{Compton} = P_e \cdot AP_{Compton} \cdot (1 - u) \cdot \sin\left(\frac{V_{CP} + \delta V_{CP}^{CIP}}{V_{\lambda/4}^{CP}} \cdot \frac{\pi}{2}\right) \cos\left(\frac{V_{PS} + \delta V_{PS}^{CIP}}{V_{\lambda/4}^{PS}} \cdot \frac{\pi}{2}\right) \quad (7)$$

where  $G$  is the photodiode gain;  $V_{CP}$  and  $V_{PS}$  are the Pockels cell voltages,  $V_{\lambda/4}$  is the Pockels cell quarter wave voltage;  $\delta V_{CP}^T$  and  $\delta V_{PS}^T$  are the laser transport phase shifts to the photodiode diagnostics;  $u$  is the amount of unpolarized light; and  $\delta V_{CP}^{CIP}$  and  $\delta V_{PS}^{CIP}$  are the laser transport phase shifts to the Compton IP. Measurements of  $PD^+$ ,  $PD^-$  and  $A_{Compton}$  are made at different Pockels cell voltages (*Pockels cell scans*) to monitor the laser transport phase shifts and the Pockels cell quarter wave voltages. This was done for the SLD Experiment, which achieved  $P_\gamma = (99.8 - 99.9)\%$  at the Compton IP with a systematic error of 0.1%. [5]

#### 4. Compton Detector and Compton Collision Rate

We plan to use a threshold Cerenkov detector, similar to that employed in the SLD Compton polarimeter [5, 6]. The detector planned for the downstream is similar to the upstream polarimeter detector. Detector R&D was reported at the Energy/Polarization workshop by D. Kaefer[7]. It is a segmented electron detector sampling the flux of scattered electrons near the kinematic endpoint. It provides a good polarization measurement with high analyzing power. The counting rate per bunch crossing is:

$$R^{eff} = R^0 \cdot \frac{l_{eff}}{l_{FWHM}} \quad (8)$$

where  $R^0$  is the rate for head on collisions,  $l_{eff}$  is the effective length of the laser bunch that collides with the (smaller) electron beam due to the crossing angle with the electron beam and  $l_{FWHM}$  is the length of the laser bunch.

$$R^{eff} = \sigma_{Compton} \cdot \frac{N_{electrons} \cdot N_{photons}}{\pi\sigma_y \cdot \sigma_x} \cdot \left[ \frac{2.35\sigma_x}{\tan \theta_{cross}} \cdot \frac{1}{l_{FWHM}} \right] \quad (9)$$

A Gaussian beam of laser light propagates as:

$$\omega(z) = \omega_0 \sqrt{1 + \left( \frac{z}{z_R} \right)^2} \quad (10)$$

The power envelope is:  $P(r) \approx e^{-\frac{2r^2}{\omega^2}}$  (11)

For an rms spot size of  $\omega_0 = 200 \mu m$  and wavelength of  $\lambda = 532 nm$  the Rayleigh range is:

$$z_R = \frac{\pi\omega_0^2}{\lambda} = 0.236m. \quad (12)$$

The distance between the lens and the Compton IP for our setup has  $z \sim 1m$  giving

$$\omega(1m) = 9.3mm.$$

We use  $N_{electrons} = 0.75 \times 10^{10}$ ;  $N_{photons} = 2.7 \times 10^{17}$  (100 mJ of 2.33 eV photons);  $\sigma_y = 150 \mu m$ ;  $\theta_{cross} = 15.44 mrad$ ;  $l_{FWHM} = 0.6m$  (corresponding to 2ns pulse length); and  $\sigma_{Compton} = 2.25 \times 10^{-31} m^2/GeV$  at the Compton endpoint (for an electron beam energy of 250 GeV and a laser photon energy of 2.33 eV). The counting rate is high with  $\sim 400$  Compton electrons per GeV at the endpoint energy of 25.2 GeV. With the current extraction line geometry, this corresponds to:

$$R^{eff} = \frac{300 \cdot scattered \cdot electrons}{cm} \cdot \left( \frac{100 \mu m}{\sigma_y} \right) \cdot \left( \frac{15.44 mrad}{\theta_{cross}} \right) \cdot \left( \frac{E_{laser}}{100 mJ} \right) \cdot \left( \frac{2n sec}{t_{FWHM}} \right) \quad (13)$$

The rate is high allowing a statistical accuracy of  $<1\%$ /minute error for each of the 3 colliding bunches in a train. During a 24 hour period all bunches of the train can be measured to less than 1% accuracy for studies of time variation within the bunch trains.

## 5. Simulation Studies

Detailed studies have been done of the Compton signal at the detector plane, as well as of possible backgrounds from the disrupted beam, beamsstrahlung and synchrotron radiation in the extraction line magnets.

## 5.1 Compton Signal

Compton scattered electrons are generated in GEANT at the Compton IP from the interaction of the extracted beam on 2.33eV laser light. In this study every beam track that reaches the Compton IP is converted into a Compton scattered electron. The distributions in energy and the vertical position,  $y$ , of the Compton scattered electrons at the Compton detector plane are shown in figure 11 for  $y > 14\text{cm}$ . The backscattered electrons have energy of 25.2 GeV and enter the Compton detector at 27.4cm.

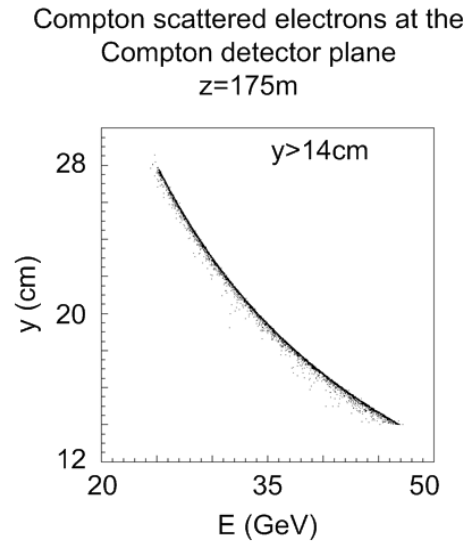


**Figure 11:** Energy versus  $y$  plot for the Compton scattered electrons at the Compton Detector plane ( $z=175\text{m}$ ).

A Cherenkov cell with horizontal width of  $\sim 1.5\text{ cm}$  will allow most of the Compton electrons to enter the detector as seen in figure 12 where  $x$  versus  $y$  is plotted. One centimeter cell size in the vertical is planned. Near the beam pipe a 1cm cell will accept about 2.5GeV (from  $\sim 44\text{GeV}$  at 15 cm to  $\sim 41.5\text{ GeV}$  at 16 cm). A 1 cm cell size accepts  $\sim 1\text{ GeV}$  near the end point energy of the backscattered electrons.

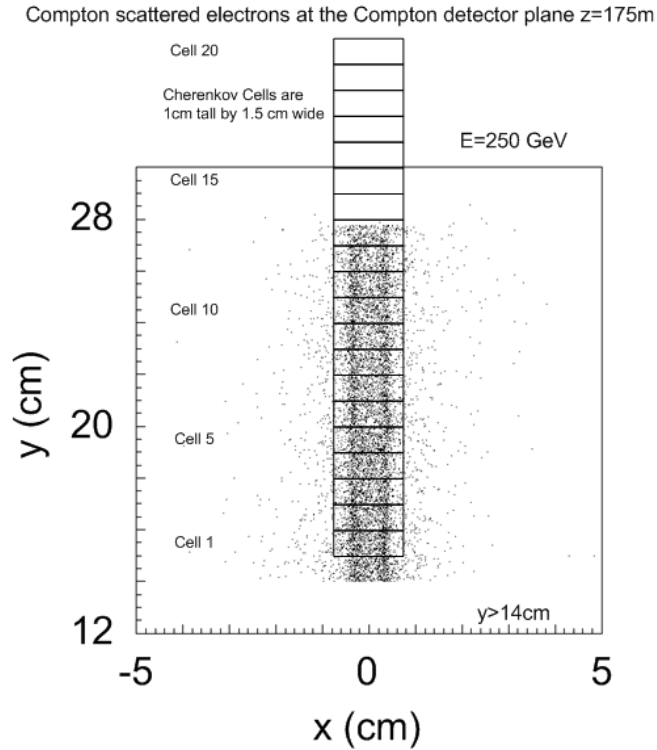


**Figure 12:** Plot of x versus y for Compton scattered electrons at the Compton Detector plane ( $z=175\text{m}$ ).

### Background Studies

Background studies have been carried out for disrupted beam losses and for synchrotron radiation. The beam losses for the nominal ILC parameter set are small and will not give significant backgrounds in the Compton Cherenkov detector. The beam losses are larger for the low power option giving a higher ILC luminosity. The low power option gives much higher beam disruption and backgrounds; Figure 13 shows the losses along the extraction beam line for this option before the location of the Compton detector.

Total loss on magnets and pipe: 152 W  
 At chicane collimators: 42 W, 2.2 W  
 At dump collimators: 2.8 kW, 6.7 kW, 10.7 kW

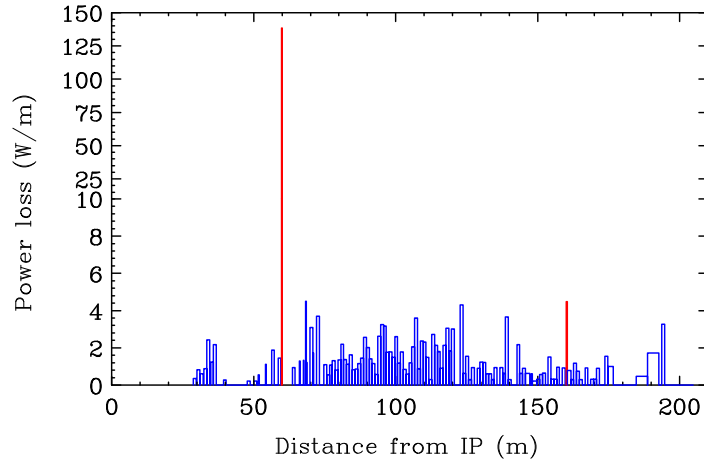


**Figure 13:** Longitudinal density of the primary beam loss for the ILC low beam power parameter option “cs14” at 250 GeV beam energy. The two red lines show loss on the energy and polarimeter chicane collimators.

Low power option cs14 tail file with  $E < 162.5$  GeV or  $\theta > 0.5$  mrad

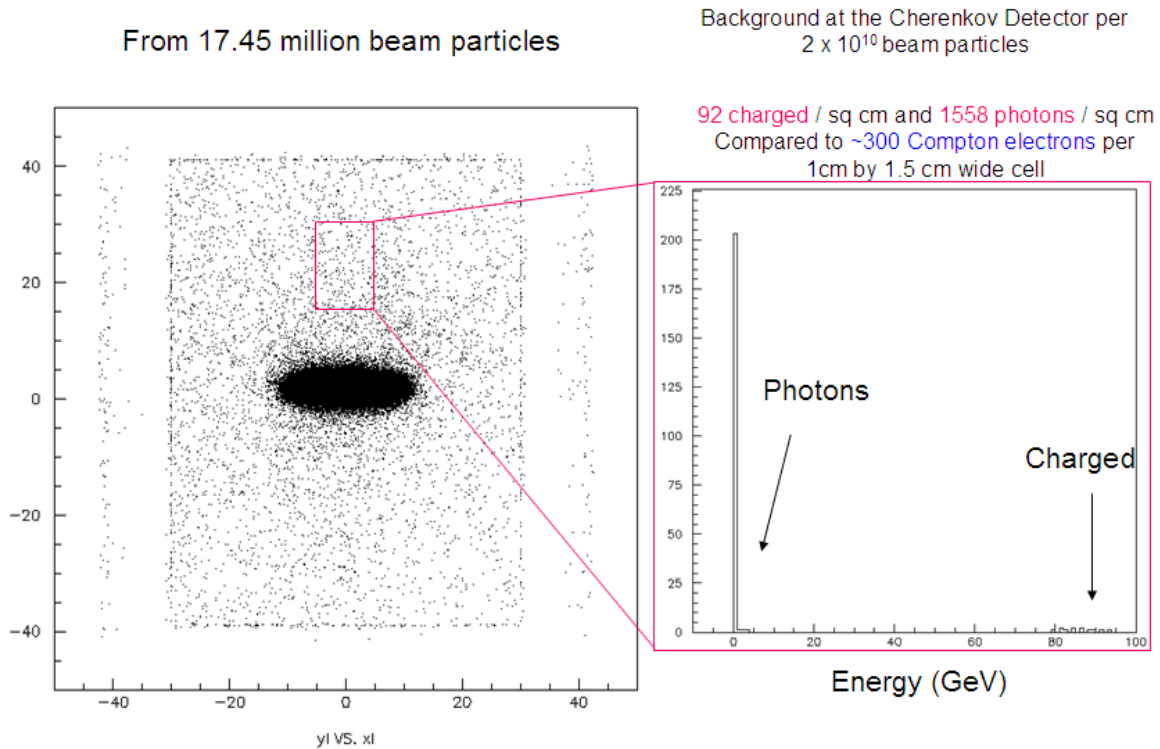


**Figure 14:** Background and beam distribution at the Cherenkov detector plane for the ILC low beam power parameter option “cs14” at 250 GeV beam energy. The plot on the right gives the energy distribution for the background particles in the area of the Cherenkov detector outlined in red.

The low energy tail of the disrupted beam in the low power option cs14 was also studied corresponding to a total 17.45 million beam particles. The study showed there will be 0.0096% lost particles between the e+e- IP and the Compton detector plane (an additional 0.00005% are lost between the Compton detector plane and z = 195 m). The lost particles produce backgrounds at the Compton detector of photons and charged particles as shown in Figure 14. Extrapolating to a beam of  $2 \times 10^{10}$  particles the backgrounds would be  $\sim 1650$  per centimeter squared (each Cherenkov cell is 1cm by 1.5cm). Most of this background is photons and only a small fraction will convert to e+e- pairs in the material before the Cherenkov detector. In addition, 56% of the background particles are photons of energy less than 15 MeV and will not give Cherenkov light. The backscattered electron counting rate is high for the proposed Compton Polarimeter with about 300 Compton electrons per 1cm by 1.5 cm Cherenkov detector cell. Therefore, we expect the backgrounds from secondary interactions to be small compared to the signal even for the Low Power beam parameter running.

A synchrotron radiation collimator protects the Compton detector and no significant SR backgrounds are expected in the Compton detector. Figure 15 shows the synchrotron radiation generated in the beam components and figure 16 shows the synchrotron radiation photons at the Compton detector plane. The sharp cutoff at 14 cm is the shadow from the special collimator located at z = 160 m shown in figure 2. There are no synchrotron radiation photons above 14.04 cm.

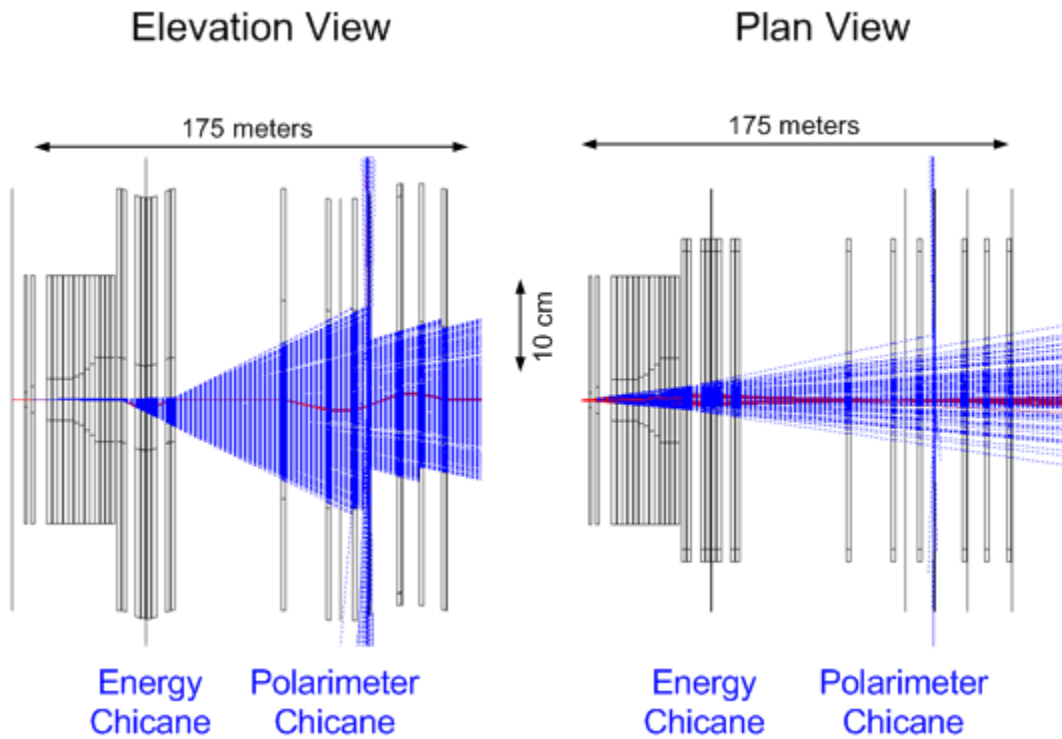


**Figure 15:** Synchrotron radiation produced by 20 beam tracks.

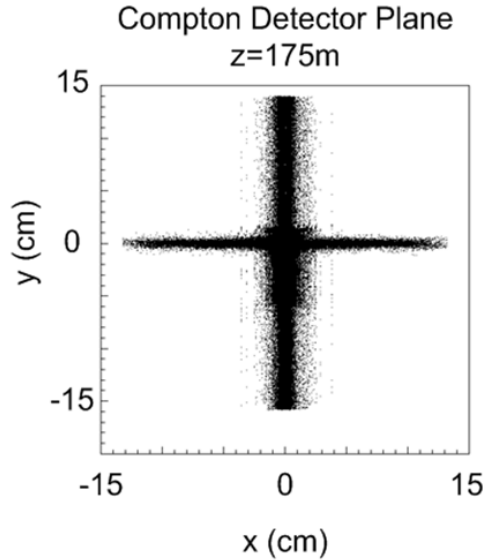


**Figure 16:** x,y distribution at the Compton detector plane of synchrotron radiation photons generated from the upstream magnets.

### 6. Polarimeter Operation at Different Beam Energies

The magnetic field of chicane magnets 3 and 4 are 1.5 times the field of magnets 1 and 2 resulting in the backscattered Compton electrons  $\sim 10$  cm further away from the beam pipe than when the four magnets all have the same magnetic field. As a result of the magnetic field difference the position of the backscattered electrons at the Cherenkov detector will move in the vertical as a function of beam energy. Figure 17 shows the trajectory of the backscattered electron when running at the Z-pole with beam energy 45.6 GeV. In this case they enter the Cherenkov detector at  $y=32.1$ cm instead of the 27.4cm for beam energy of 250 GeV. Figure 18 shows in the plot on the left the position of the backscattered Compton electrons for different beam energies when magnets 3 and 4 have 1.5 times the field of magnets 1 and 2 of the polarimeter chicane. The plot on the right shows the scaling multiplier of the last two dipoles to keep the Compton edge at 27.4cm from the beam line independent of beam energy.

## Polarimeter Chicane

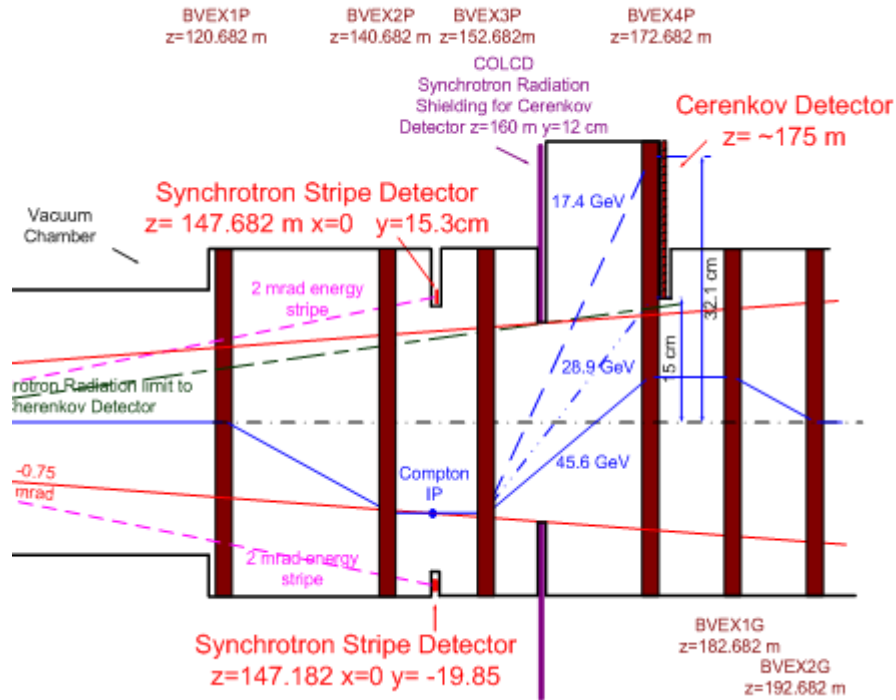


**Figure 17:** Diagram of the Polarimeter Chicane at Z-pole center of mass energy with beam at 45.6 GeV.

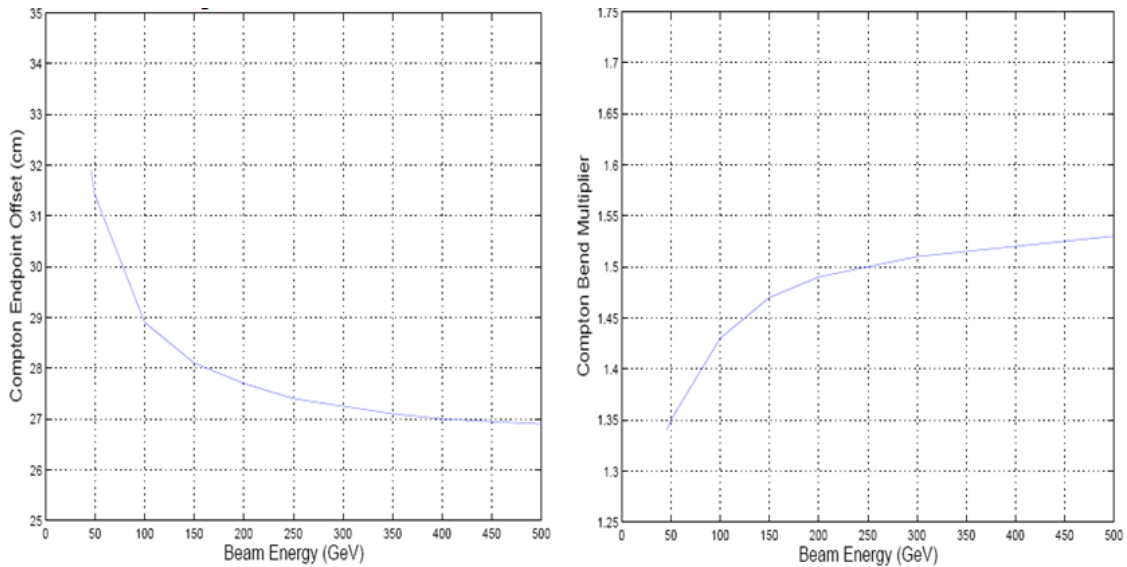


**Figure 18:** Plot on the left shows the vertical offset of the Compton endpoint at the Compton detector plane for a fixed-field chicane with 20mm dispersion at 250GeV and the last 2 polarimeter chicane magnets with 50% stronger field than the first two magnets. Plot on the right shows the scaling multiplier of the last two dipoles to keep the Compton edge at 27.4cm from the beam line independent of beam energy.

## 7. Conclusions

The downstream polarimeter in the extraction line of the ILC will operate with high precision of 0.25% from the Z-pole center of mass energy to the highest ILC energies available of 1 TeV. The acceptance of the Compton Cherenkov detector covers a large part of the Compton electron energy spectra with the backscattered electrons more than 10 cm from the ILC vacuum pipe. Backgrounds from synchrotron radiation produced upstream of the Cherenkov detector and from lost particles along the beam line are small compared to the Compton scattered electron signal.

Future studies needed include: i) backgrounds from beam gas interactions and beam losses from a realistic vacuum chamber design, and ii) a detailed design for the laser entrance and exit with movable Compton IP at different beam energies.

## References

- [1] M. L. Swartz, Phys.Rev. D58 (1998) 014010. [hep-ph/9711447]
- [2] ILC Global Design Effort and World Wide Study, Editors: N. Phinney, N. Toge and N. Walker, “International Linear Collider Reference Design Report”, AUGUST, 2007
- [3] K. Moffeit, et al, “Proposal to modify the polarimeter chicane in the ILC 14 mrad extraction line”, SLAC-PUB-12425, IPBI TN-2007-1, March 2007
- [4] Description of Continuum Powerlite 8000 lasers found at [www.continuumlasers.com](http://www.continuumlasers.com).
- [5] K. Abe et al., SLD Collaboration, Phys. Rev. Lett. **70**, 2515 (1993); K. Abe et al SLD Collaboration., Phys. Rev. Lett. **8678**, 11622075 (20011997); R. Elia, SLAC-Report-429 (1994); R. King, SLAC-Report-452, 1994; A. Lath, SLAC-Report-454, 1994; E. Torrence, SLAC-Report-509, 1997. The technical description of the laser light source for the SLD experiment found in the thesis cited here have been used for some parts of this publication.
- [6] M. Woods, SLAC-PUB-7319, 1996, e-Print Archive: **hep-ex/9611005**.
- [7] D. Kaefler, “Prototype Design for the Cherenkov Detector”, DESY-FLC, April 2008. <https://indico.desy.de/getFile.py/access?contribId=22&sessionId=8&resId=0&materialId=paper&confId=585>